ACS Energy LETTERS

Cite This: *ACS Energy Lett.* 2019, 4, 2205−2212

http://pubs.acs.org/journal/aelccp

Role of Electron−Phonon Coupling in the Thermal Evolution of Bulk Rashba-Like Spin-Split Lead Halide Perovskites Exhibiting Dual-Band Photoluminescence

Julian A. Steele,[*,†] Pascal Puech,[‡] Bartomeu Monserrat,[§] Bo Wu,[∥] Ruo Xi Yang,[⊥] Thomas Kirchartz,[#,∇] Haifeng Yuan,[○] Guillaume Fleury,[†] David Giovanni,[◆] Eduard Fron,[○] Masoumeh Keshavarz,[○] Elke Debroye,[○] Guofu Zhou,[∥] Tze Chien Sum,[◆] Aron Walsh,[¶,&] Johan Hofkens,[○] and Maarten B. J. Roeffaers[*,†]

[†]cMACS, Department of Microbial and Molecular Systems, KU Leuven, Celestijnenlaan 200F, 3001 Leuven, Belgium

[‡]CEMES/CNRS, Université de Toulouse, 29, rue Jeanne Marvig, 31055 Toulouse, France

[§]TCM Group, Cavendish Laboratory, University of Cambridge, J. J. Thomson Avenue, Cambridge CB3 0HE, United Kingdom

[∥]Guangdong Provincial Key Laboratory of Optical Information Materials and Technology & Institute of Electronic Paper Displays, South China Academy of Advanced Optoelectronics, South China Normal University, Guangzhou 510006, People's Republic of China

[⊥]Molecular Foundry, Lawrence Berkeley National Laboratory, 1 Cyclotron Road, Berkeley, California 94720, United States

[#]IEK5-Photovoltaics, Forschungszentrum Jülich, 52425 Jülich, Germany

[∇]Faculty of Engineering and CENIDE, University of Duisburg−Essen, Carl-Benz-Straße 199, 47057 Duisburg, Germany

[○]Department of Chemistry, KU Leuven, Celestijnenlaan 200F, 3001 Leuven, Belgium

[◆]Division of Physics and Applied Physics, School of Physical and Mathematical Sciences, Nanyang Technological University, 21 Nanyang Link, Singapore 637371, Singapore

[¶]Department of Materials, Imperial College London, Exhibition Road, London SW7 2AZ, United Kingdom

[&]Global E3 Institute and Department of Materials Science and Engineering, Yonsei University, Seoul 120-749, Korea

Supporting Information

ABSTRACT: The optoelectronic properties of lead halide perovskites strongly depend on their underlying crystal symmetries and dynamics, sometimes exhibiting a dual photoluminescence (PL) emission via Rashba-like effects. Here we exploit spin- and temperature-dependent PL to study single-crystal $APbBr_3$ (A = Cs and methylammonium; CH_3NH_3) and evaluate the peak energy, intensity, and line width evolutions of their dual emission. Both perovskites exhibit temperature trends governed by two temperature regimes—above and below approximately 100 K—which impose different carrier scattering and radiative recombination dynamics. With increasing temperature, high-energy optical phonons activate near 100 K to drive energy splitting of the dual bands and induce line width broadening via electron−phonon coupling, with a stronger coupling constant inferred for carriers recombining by the spin-split indirect bands, compared to the direct ones. We find that the unusual thermal evolutions of all-inorganic and hybrid bulk lead bromide perovskites are comparable, suggesting A-site independence and the dominance of dynamic effects, and are best understood within a framework that accounts for Rashba-like effects.

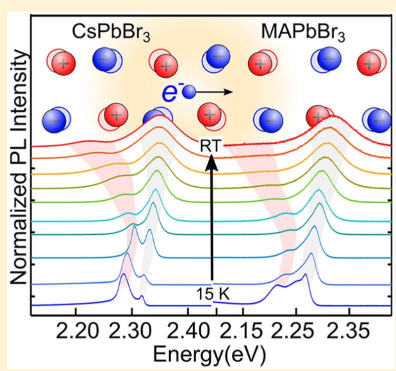

The interest for solution-processable lead halide perovskites within efficient solar cells[1,2] stems from their promising optoelectronic response to sunlight and high tolerance to defects.[3,4] This family of semiconductors is increasingly being considered as "soft" solid-state materials,[5−7]

Received: July 3, 2019
Accepted: August 19, 2019
Published: August 19, 2019

DOI: 10.1021/acsenergylett.9b01427
ACS Energy Lett. 2019, 4, 2205−2212

whereby the fate of photogenerated charges primarily relies on the fundamental carrier−lattice interaction dynamics. For instance, polaron formation—via carrier−longitudinal optical phonon (Fröhlich) interactions—within the lattice has been linked to several favorable qualities, like long carrier lifetimes and diffusion lengths.[8−10] Recent indications of spin splitting and indirect tail state formation in lead halide perovskites[11−16] due to Rashba-like effects[17] motivate a reconsideration of how electron−phonon coupling can exist within its perturbed electronic band structure. Universally, for the application of any polar metal halide perovskite, the properties of the free charge carriers and phonon scattering mechanisms are central to its optoelectronic performance at room temperature (RT).

Bulk Rashba-like effects occur in metal halide perovskites via two key ingredients. First, heavy elements, like Pb, introduce strong spin−orbit coupling (SOC) into the electronic structure. Second, the crystal must lack inversion symmetry, so that an effective magnetic field is imposed on electrons by SOC, lifting spin degeneracy and splitting the band electronic structure (Figure 1). To lose inversion symmetry, both static[18] (i.e., intrinsically noncentrosymmetric) and dynamic[12,13,19] (i.e., fluctuating local breaks in symmetry) mechanisms have been proposed, though the full picture is still debated.[20] Consequently, the valence band maxima[21] (VBM) and conduction band minima (CBM) shift away from the high-symmetry points in the Brillouin zone, giving rise to low-energy (LE) indirect tail states[11,15] (Figure 1). The shift for Pb-based perovskites in reciprocal space is expected to be larger for the CBM compared to that for the VBM due to the relative orbital contributions to the band structure,[22] producing a LE indirect transition alongside a high-energy (HE) direct one. Notably, these phenomena constitute a general result within both all-inorganic and hybrid lead halide perovskites, leading to a characteristic dual photoluminescence (PL) emission[11,15] that is better seen at low temperatures.[23]

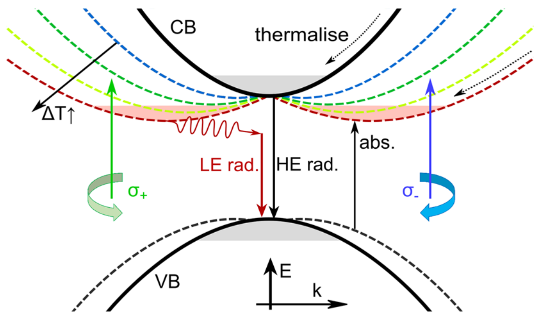

Figure 1. Schematic of energy band structure experiencing thermally driven Rashba-like spin splitting, with selective excitation provided using left (σ_+) and right (σ_-) circularly polarized light. Photogenerated carriers recombine by two main radiative (rad.) pathways, a HE unperturbed direct bandgap transition and a phonon-mediated low-energy (LE) indirect bandgap. For simplicity, only the CB splitting shows a thermal dependence.

The origin of the spin splitting in bulk hybrid lead halide perovskites like $MAPbBr_3$ (where MA is methylammonium; CH_3NH_3) is unclear and is especially puzzling for all-inorganic $CsPbBr_3$, which adopts a centrosymmetric orthorhombic (*Pnma*) crystal structure[24] at RT. However, it is expected that the thermal motion of the Cs^+ atoms (as well as MA molecules) at the cation A-sites couples to lattice vibrations to promote local polar fluctuations[25] (Figure 2a inset) and dynamically break local centrosymmetry.[13,16] It is not known if $CsPbBr_3$ or $MAPbBr_3$ adopt a "static" centrosymmetric structure near 0 K.[11] The intensity of the Rashba-induced LE peak is sensitive to sample preparation,[11] being best resolved in large single crystals (SCs).[26] As such, PL-based studies[27,28] become ambiguous when comparing across different physical microstructures, i.e., nanocrystals or polycrystalline networks. Nevertheless, accounting for Rashba-like effects that underpin the low-temperature dual PL emission in $CsPbBr_3$ and $MAPbBr_3$ will yield a more accurate description of the photophysics involved.[29,30]

In this Letter, we report a spin- and temperature-dependent PL analysis of the emission positions, line widths, and intensities arising in SC all-inorganic $CsPbBr_3$ and hybrid $MAPbBr_3$ perovskites possessing dual bands at RT. The two systems exhibit a comparable dependence on temperature, inferring that the underlying models employed are cation-

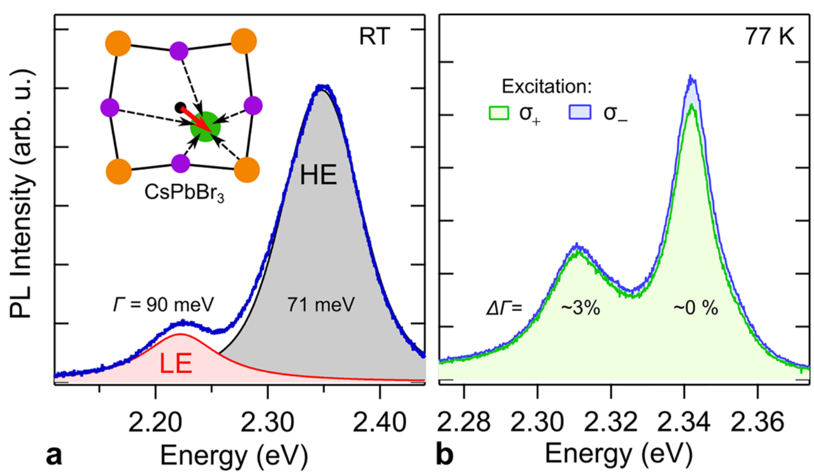

Figure 2. (a) RT PL spectrum of SC $CsPbBr_3$ ($\lambda_{exc.}$= 400 nm) with dual HE and LE emissions, with their fwhm (Γ) indicated. The inset illustrates how the perovskite "cage" (Pb−Br framework) and dynamic symmetry breaking[13] of an off-center Cs cation (green) create an effective electric dipole moment (solid red arrow) through the summation of local dipoles (dashed arrows). (b) Right circularly polarized PL spectra (77 K) of $CsPbBr_3$ upon exciting (473 nm) with left (σ_+) and right (σ_-) circularly polarized light. The ΔΓ values depict the difference in the line width derived from their fitting: $\Delta\Gamma = 2[\Gamma(\sigma_-) - \Gamma(\sigma_+)]/[\Gamma(\sigma_-) + \Gamma(\sigma_+)]$.

DOI: 10.1021/acsenergylett.9b01427
ACS Energy Lett. 2019, 4, 2205−2212

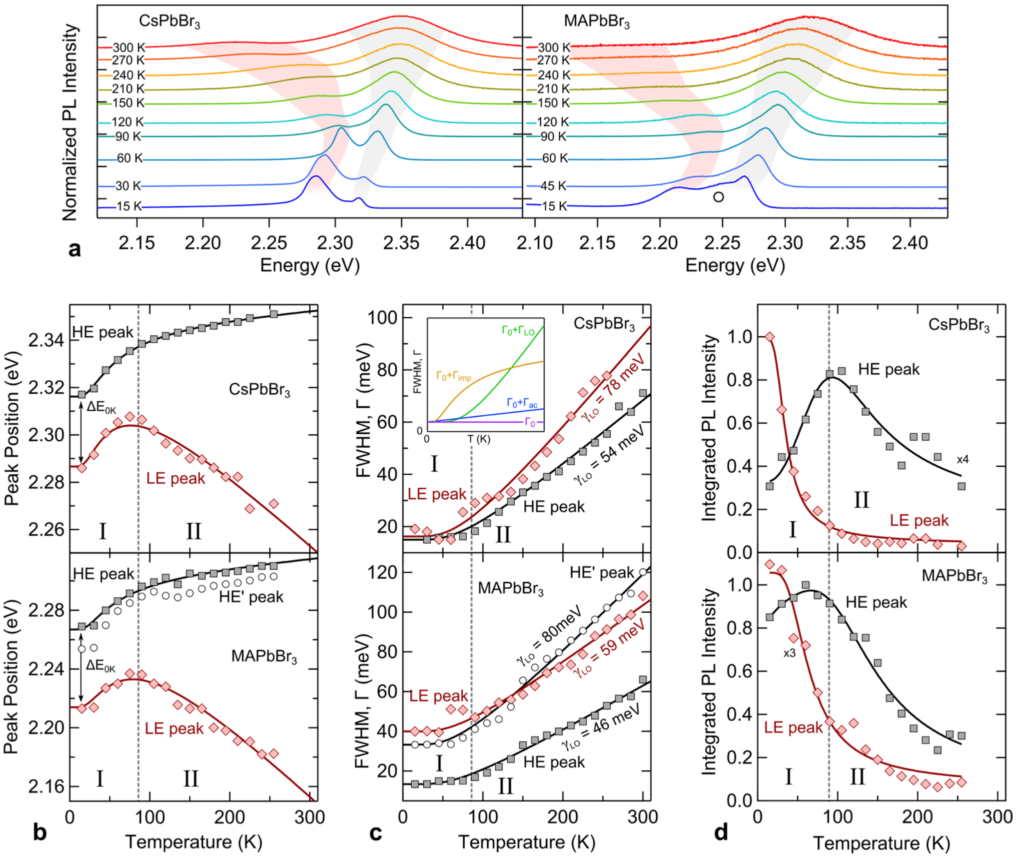

Figure 3. (a) Normalized low-temperature PL spectra of SC $CsPbBr_3$ and $MAPbBr_3$ ($\lambda_{exc.}$ = 400 nm/3.1 eV), with the open circle in the $MAPbBr_3$ data set highlighting the phonon replica peak (HE′) at low-temperatures. Analysis of the temperature evolution for both material systems: (b) Emission peak energies modeled using eq 3, including the feature identified in (a) by the open circle; (c) fwhm of the dual bands fit via eq 5; (d) normalized integrated LE and HE peak intensities, fit using eqs 6 and 7, respectively. For $MAPbBr_3$, the integration of HE includes the signal of its satellite peak. For each analysis, low-temperature and high-temperature trends are respectively identified by regimes I and II. The inset in (c) shows the archetypal form of the temperature dependence of each contributing term in eq 5.

independent and are strongly driven by lattice dynamics. The LE and HE peak positions undergo different evolutions in the lead bromide perovskites, whereby both peaks blue shift when warming above 0 K, with LE undertaking an additional strong red shift above 100 K, with the activation of optical phonons. While high-temperature quenching of the LE emission intensity is in line with typical semiconducting behavior, we assign thermal-driven intersystem crossing to account for a HE intensity that peaks near 100 K and quenches when approaching 0 K. The Fröhlich coupling strength of carriers residing in the spin-split bands is found to be much higher than that in the direct bands in $CsPbBr_3$, inferred from the temperature-dependent line width broadening. We demonstrate that several anomalous features in the low-temperature dual PL emission evolution found in SC $CsPbBr_3$ and $MAPbBr_3$ are best understood when Rashba-like effects are considered.

$APbBr_3$ (A = Cs and MA) SCs were prepared with a modified recipe from the literature,[31] resulting in 1−3 mm sized perovskite SCs (Methods and Figure S1 of the Supporting Information). Figure 2a provides the RT PL spectrum of $CsPbBr_3$, displaying a clear dual emission.[11] At RT, the emission full width at half-maximum (fwhm: Γ) will be dominated[32] by the Fröhlich interaction strength, represented by dimensionless constant α, which scales with the carrier effective mass (m^*) according to the Feynman polaron model[33] as

$$\alpha = \frac{e^2}{\hbar c}\sqrt{\frac{m^* c}{2\hbar\omega_{LO}}}\left(\frac{1}{\varepsilon_\infty} - \frac{1}{\varepsilon_0}\right) \tag{1}$$

Parameters ε_∞ and ε_0 respectively indicate the high-frequency and static dielectric constants, c is the speed of light, $\hbar$ is the reduced Planck constant, e is the fundamental charge, and ω_{LO} is the frequency of the coupling optical phonon mode(s) involved. The decisive factor for m^* is the $E-k$ dispersion curvature at the CB and VB extrema (assuming near-parabolic character), whereby $m^*(k) \propto (\partial^2E/\partial k^2)^{-1}$.

Within the spin-split system depicted in Figure 1, a one-band effective mass approximation no longer holds[34] for eq 1, given that two shallow side valleys are formed. For example, carriers thermalizing into each Rashba-induced valley will have nontrivial spin texture, with intervalley scattering mediated via phonons. Importantly, for the spin-split bands, their curvature is expected to be small compared to the direct transition,[19,35] indicating an increase in the effective mass and a relative increase of the Fröhlich interaction. In Figure 2a, the line width of LE is relatively larger than that of HE at RT.

The effective mass of charges in the two spin-split indirect bands will evolve as a function of the SOC, described by the Rashba Hamiltonian.[34] Both the electron−phonon coupling[36,37] and the (large) polaronic effective mass[38] correction

DOI: 10.1021/acsenergylett.9b01427
ACS Energy Lett. 2019, 4, 2205−2212

are enhanced by Rashba-like effects. In this scenario, the relative electron−phonon coupling strength for the carrier in the lower (−) Rashba band are expected to be larger than that in the upper (+) one.[38] As a result, carriers recombining at the two spin-split band edges will encounter different polaron effects, leading to stronger coupling and a broader PL emission arising from recombination via the lower branch. We experimentally assess this via a comparison of the LE emission fwhm (Γ) when the recombination has different spin populations, down at cryogenic temperatures (T = 77 K) where the LE band is more pronounced. To exclude instrumental response to light helicity, we fixed the detection optics and only vary the incident polarization. Figure 2b displays right circularly polarized PL spectra recorded from $CsPbBr_3$ using left (σ_+) and right (σ_-) circularly polarized excitation. Beyond the polarization dependence of the emission intensities,[11] fitting these data (Voigt functions) reveals an approximately 3% broader LE peak using σ_- excitation compared to σ_+, with no detectable change in the HE line width. While this difference is relatively small (the indirect recombination rate will occur relatively slowly compared to the rate of spin-flipping), it is consistent with a relative disparity in the electron−phonon coupling arising from the two spin valleys and should be enhanced exciting closer to the split band edges.[11]

Smearing the spin information, Figure 3a overviews the unpolarized temperature dependence of the normalized PL line shape recorded from SC $CsPbBr_3$ and $MAPbBr_3$ (raw spectra shown in Figure S2). A lower energy shoulder on the $MAPbBr_3$ HE peak appears and grows at relatively low temperatures, a feature that is location-dependent on the crystal surface (Figure S3). Fitting the HE band of $MAPbBr_3$ with an additional peak reveals this feature to closely track the thermally driven energy shift of HE (Figure 3b) and is respectively red shifted by ∼15 meV (at lower temperatures where it is better resolved). The paralleled evolution and the relative energy shift (i.e., close to the characteristic optical phonon energies[39]) of this peak are consistent with the formation of a red shifted satellite band, attributable to phonon replicas[40,41] (identified as HE′). While similar behavior is not exhibited in the SC $CsPbBr_3$ PL emission, their overall thermal evolutions are fairly comparable[42] and are thus evaluated together.

The LE and HE peak positions undergo different evolutions in Figure 3b, due to the superposition of two identified trends. Trend I raises the energy of both peaks due to a blue shift in the absorption edge with increasing temperature, driven by a combination of thermal expansion and electron−phonon coupling.[37,43,44] LE experiences an additional red shift in regime II at higher temperatures, representing a thermally induced band splitting[11] superimposed on the aforementioned blue shift. Both effects are activated by phonons with "effective" vibrational energies ($\hbar\omega$)—via electron−phonon coupling—although the respective modes involved are very different. For instance, any phonon mode (acoustic or optical) can raise the lead halide perovskite bandgap energy with increasing temperature;[27,37] however, high-temperature Rashba-like effects must involve modes that break local inversion symmetry.[19]

The respective phonon population is governed by Bose−Einstein statistics

$$n(T) = \frac{1}{e^{\hbar\omega/k_B T} - 1} \tag{2}$$

where k_B is the Boltzmann constant. Warming above 0 K, low-frequency acoustic phonons dominate the initial rise in bandgap energy.[27,37,45] At higher temperatures, optical phonons and spin splitting become more influential, inverting the relative shift in LE.[11] This infers that trend I needs only relatively low phonon energies, while trend II requires relatively high frequency modes.

Considering the interaction of electrons with the crystal lattice, the temperature dependence of the emission peaks can be reduced to the Bose−Einstein bandgap model[46,47]

$$E(T) = E_0 + \sum_i A_i\left(\frac{1}{e^{\hbar\omega_i/k_B T} - 1} + \frac{1}{2}\right) \tag{3}$$

For up to three Bose−Einstein oscillators ω_i (i = 1, 2, 3), A_i represents their weight, which if negative (positive) describes the degree of the energy decrease (increase) with rising temperature, and E_0 is the bandgap energy at 0 K. The evolution of high-frequency will involve the summation of a low-frequency acoustic phonon branch (i = 1) and a higher-energy optical phonon one (i = 2), with opposite weightings. LE initially follows the shift of high-frequency, though it is red shifted by a third relatively high-frequency oscillator (i = 3) during trend II. Therefore, the two Bose−Einstein terms used to account for HE are used as inputs to evaluate their combined influence on LE (fitting parameters in Table S1). The effective phonon frequencies shifting HE ($CsPbBr_3$: $\hbar\omega_1$ = 3.8 meV, $\hbar\omega_2$ = 7.0 meV; $MAPbBr_3$: $\hbar\omega_1$ = 3.6 meV, $\hbar\omega_2$ = 6.4 meV) are estimated to be far smaller than the phonons driving the LE red shift ($CsPbBr_3$: $\hbar\omega_3$ = 14.7 meV; $MAPbBr_3$: $\hbar\omega_3$ = 11.3 meV). We note the potential involvement of Raman-active optical modes nearing this energy (Figures S4 and S5), whose population will be relatively small below 100 K, in line with the two different regimes identified in the model. Interestingly, the HE and LE peaks in Figure 3b approach an intrinsic energy split near zero temperature;[11] ΔE_{0K} = 30 meV for $CsPbBr_3$, while ΔE_{0K} = 55 meV for $MAPbBr_3$. While dynamic effects arising from thermal fluctuations are suppressed with decreasing temperature, this does not mean that all dynamic effects vanish in quantum systems. Even at absolute zero there are dynamic fluctuations arising from quantum zero-point motion. This comes from predictions made for the perovskites under consideration[19] and are based on the intrinsic dynamic disorder and peak energy splitting at 0 K. More generally, quantum zero-point fluctuations are known to play a major role in other perovskite materials, with the best known example being $SrTiO_3$, which is a quantum paraelectric in which quantum fluctuations stabilize the paraelectric phase compared to the ferroelectric phase.[48] Alternatively, in the absence of clear structural data for these materials near 0 K, the energy split may potentially come about by a loss of centrosymmetry in the local crystal structure. However, because the dual peak evolution is common to both all-inorganic $CsPbBr_3$ and hybrid $MAPbBr_3$ materials, this result reinforces the interpretation of "dynamical" spin splitting in the Cs case as MA statically breaks inversion symmetry due to its dipole, whereas Cs should not statically break inversion symmetry (i.e., spherical atom). The paralleled behavior of both systems shows that with the inclusion of dynamics the physics becomes the same and is in all cases dominated by the dynamical spin splitting.

DOI: 10.1021/acsenergylett.9b01427
ACS Energy Lett. 2019, 4, 2205−2212

Assessing the temperature-dependent emission broadening in Figure 3c, the intrinsic fwhm's (Γ_0) of both perovskites grow with increasing temperatures. In Figure 3c, the LE emission from both $CsPbBr_3$ and $MAPbBr_3$ broadens faster than HE with rising temperature, suggesting enhanced carrier scattering in these bands. The temperature-dependent excitonic line width of band-to-band transitions within semiconductors[32,49] is relatively well understood, being described by

$$\begin{aligned}\Gamma(T) &= \Gamma_0 + \Gamma_{ac} + \Gamma_{LO} + \Gamma_{imp} \\ &= \Gamma_0 + \gamma_{ac}T + \gamma_{LO}n(T) + \gamma_{imp}e^{-E_b/k_BT}\end{aligned} \tag{4}$$

The second and third terms (Γ_{ac} and Γ_{LO}) respectively describe the trends ascribed to acoustic and LO-phonon (Fröhlich) scattering, with coupling strengths γ_{ac} and γ_{LO}. The fourth term accounts for the scattering from ionized impurities, with average binding energy E_b. Below 75 K, the linear Γ_{ac} component—involving lower energy acoustic phonons—will dominate the broadening. The gradient of the of the fwhm of all peaks is relatively flat in regime I, in line with negligible contributions from the γ_{ac} term,[32,50−52] and is omitted for simplicity. The small sublinear feature in LE below 100 K for both $CsPbBr_3$ and $MAPbBr_3$ resembles the influence of Γ_{imp} (inset of Figure 3d) but does not appear in HE. Because it is unlikely that ionized impurities will selectively scatter carriers residing only in the LE bands, this feature is suggested to have other origins, and we omit it for simplicity.[32] There is a group of distinct LO-optical vibrations expected to interact with charge carriers[53] (Figures S4 and S5) in lead bromide perovskites with energies close to 17 meV (~140 cm^{-1}). As well, the energy of the optical phonon band is stable down to cryogenic temperatures. Therefore, we adopt a simplified model to fit our data,[32] dependent on two dominant components

$$\Gamma(T) = \Gamma_0 + \frac{\gamma_{LO}}{e^{\hbar\omega_{LO}/k_BT} - 1} \tag{5}$$

For the LE band, a temperature-invariant γ_{LO} broadening parameter may not fully describe its behavior over the temperature range explored as its nature depends on the phonon population. However, the broadening of LE above 100 K is fairly linear in both $CsPbBr_3$ and $MAPbBr_3$, being agreeably fit by a fixed γ_{LO} parameter. We note that analogous models have been used for heavy- and light-hole VB splitting in strained epitaxial semiconductors and quantum wells,[54] which experience temperature-dependent changes in their band dispersion at the high-symmetry points.

Through eq 5, we estimate the relative strength of the Fröhlich coupling arising in the two recombination pathways in $CsPbBr_3$; γ_{LO} is revealed to be 54 ± 5 meV for the direct HE transition and 78 ± 8 meV from the LE line width broadening. Likewise, for $MAPbBr_3$, γ_{LO} is determined to be 46 ± 3 and 59 ± 6 meV for HE and LE, respectively, and relatively larger at 80 ± 10 meV for the HE′ satellite. The large difference in coupling strength between the direct HE and spin-split LE emissions from both of these perovskites is expected within a phonon-driven broadening model that corrects for SOC, i.e., making the Rashba-induced LE band broaden faster, via stronger Fröhlich coupling. However, the sensitivity of the LE emission to the sample preparation[11] may explain the large spread in γ_{LO} values reported[32,51,52,55−58] from low-temperature PL analysis of these materials, reaching as high as 130 meV.[59]

Figure 3a shows that the relative weighting of the normalized LE band significantly grows for both SC $CsPbBr_3$ and $MAPbBr_3$ perovskites upon cooling, which is tracked in Figure 3d (note that the $MAPbBr_3$ HE intensity is derived from the combined integrated emission of both HE and HE′ bands). First, considering the more standard characteristic of the LE bands, the initial intensity (I_0) decreases above 0 K due to thermally activated quenching (estimated via a single dominant nonradiative channel), commonly described by an Arrhenius expression

$$I(T) = \frac{I_0}{1 + ae^{-E_a/k_BT}} \tag{6}$$

where a is the ratio of nonradiative and radiative probabilities and E_a is the activation energy of the quenching channel. Applying eq 6 to the temperature dependence of the LE intensity yields an activation energy of 11 meV for $CsPbBr_3$ and 18 meV for $MAPbBr_3$ (Table S2).

The temperature dependence of the HE emissions, on the other hand, is more complex; the HE peak intensity maximizes near 90 K and begins to quench moving to either lower (regime I) or higher (regime II) temperatures. At higher temperatures, the HE intensity decrease is similar to that of LE, manifesting via indiscriminate thermally activated nonradiative carrier recombination. In regime I, however, the system is subject to another nonradiative channel that becomes more significant upon approaching 0 K. The Arrhenius fitting can be modified to include the second quenching term, whereby

$$I(T) = \frac{I_0}{1 + a_1e^{-E_{a1}/k_BT} + a_2e^{-E_{a2}/k_BT}} \tag{7}$$

The two competing processes ($a_1 > 0$; $a_2 < 0$) superimpose to yield a maximum below 100 K, with the fitting parameters provided in Table S2.

The origin of the nonradiative channel quenching in regime I for both $CsPbBr_3$ and $MAPbBr_3$ is difficult to isolate, though it is likely connected to thermally driven intersystem crossing between the bright LE spin-split triplet states and the bright direct transition involving a singlet state.[60] This is because the intersystem crossing between the states is mediated by optical phonons, which are depopulated and disappear toward 0 K. On the basis of the predicted exciton fine structure of $CsPbBr_3$ perovskite,[60−63] an energy scheme representing this proposition is displayed in Figure 4. The left and right portions of the scheme represent the static and dynamic cases of the electronic structure, which generate the unperturbed and perturbed band structures in Figure 1, respectively. As shown in Figure 4, thermal energy is required to populate the LE Rashba bands and allow intersystem crossing to the static HE states, thus facilitating a more intense HE emission. This is because the band structure remains split at 0 K, retaining the lower-energy indirect tail states shown in Figure 1. That is to say, some of the rise in the LE emission intensity while cooling in regime I is at the cost of depopulating the radiative HE transition.

In summary, we have reported a low-temperature PL analysis of high-quality SCs of $CsPbBr_3$ and $MAPbBr_3$ emitting a dual emission accounting for Rashba-like effects. The thermal evolution of the two perovskites—one being an all-inorganic system and the other a hybrid—are very comparable, suggesting that the underlying physics of the temperature

DOI: 10.1021/acsenergylett.9b01427
ACS Energy Lett. 2019, 4, 2205−2212

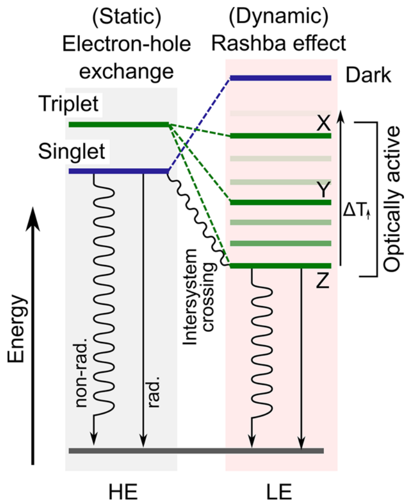

Figure 4. Expected fine structure[60] of the band-edge excitons considering short- and long-range electron−hole exchange (left) and then including Rashba-like effects[61] with dynamic symmetry breaking along the *z* direction (right), under orthorhombic symmetry. In the split states (dynamic), the exciton separates into three bright states and a higher energy dark state. Intersystem crossing will depend on the relative population of the LE spin-split triplet states, which is governed by the crystal temperature.

dependence is cation-independent and dominated by dynamics, in line with recent predictions. We find that a single-band-to-band model no longer accounts for the radiative recombination pathways expressed in $APbBr_3$ perovskites due to different physical properties of carriers residing in the split band structure. While the formation of indirect tail states promotes longer radiative lifetimes,[14] it ultimately enhances electron−phonon scattering, reducing carrier mobility, and leads to a relatively broad LE emission. To explain the origin of this behavior, we connect both the enhancement in the effective mass of carriers residing in the spin-split bands and the requirement for additional scattering to overlap the bands for recombination. Further, the direct band-edge recombination is quenched near 0 K, which we attribute to the presence of an unpopulated LE indirect emission pathway. These findings allow rationalization of previous experimental observations and provide a key to understanding the complex carrier dynamics in bulk spin-split halide perovskites.

■ ASSOCIATED CONTENT

Supporting Information

The Supporting Information is available free of charge on the ACS Publications website at DOI: 10.1021/acsenergylett.9b01427.

Experimental methods and additional figures and tables showing powder XRD scans, non-normalized temperature-dependent PL spectra, comparison of location-dependent PL spectra, temperature-dependent first-order Raman scattering spectra, and fitting parameters (PDF)

■ AUTHOR INFORMATION

Corresponding Authors

*E-mail: julian.steele@kuleuven.be.
*E-mail: maarten.roeffaers@kuleuven.be.

ORCID

Julian A. Steele: 0000-0001-7982-4413
Thomas Kirchartz: 0000-0002-6954-8213
Haifeng Yuan: 0000-0001-6652-3670
Guillaume Fleury: 0000-0001-9480-3952
Eduard Fron: 0000-0003-2260-0798
Masoumeh Keshavarz: 0000-0003-3685-6778
Elke Debroye: 0000-0003-1087-4759
Guofu Zhou: 0000-0003-1101-1947
Tze Chien Sum: 0000-0003-4049-2719
Aron Walsh: 0000-0001-5460-7033
Johan Hofkens: 0000-0002-9101-0567

Notes

The authors declare no competing financial interest.

■ ACKNOWLEDGMENTS

The authors acknowledge financial support from the Research Foundation-Flanders (FWO, Grant Nos. 12Y7218N, G.0197.11, 12Y6418N, and 12O3719N postdoctoral fellowship to J.A.S., H.Y., M.K., and E.D.), KU Leuven Research Fund (C14/15/053), the Flemish government through long term structural funding Methusalem (CASAS2, Meth/15/04), the Hercules foundation (HER/11/14), and the Belgian Federal Science Policy Office (IAP-VII/05). The research leading to these results has received funding from the European Research Council under the European Union's Seventh Framework Programme (FP/2007-2013)/ERC Grant Agreement (Grant No. 307523). B.M. acknowledges support from the Winton Programme for the Physics of Sustainability and from Robinson College, Cambridge, and the Cambridge Philosophical Society for a Henslow Research Fellowship. B.W. acknowledges support from the National Natural Science Foundation of China (NFSC) (Grant No. 51802331), Guangdong Provincial Key Laboratory of Optical Information Materials and Technology (Grant No. 2017B030301007), and the 111 Project. T.K. acknowledges support from the Impuls- und Vernetzungsfonds der Helmholtz Gemeinschaft via the project PEROSEED. We are grateful to the UK Materials and Molecular Modelling Hub for computational resources, which is partially funded by EPSRC (EP/P020194/1). T.C.S. and D.G. acknowledge the support from the Ministry of Education AcRF Tier 2 Grant MOE2016-T2-1-034 and MOE2017-T2-1-001 and from the Singapore National Research Foundation Investigatorship NRF-NRFI-2018-04. We would also like to express our sincere thanks to Prof. Chao Zhang for his helpful discussions.

■ REFERENCES

(1) Green, M. A.; Ho-Baillie, A.; Snaith, H. J. The emergence of perovskite solar cells. *Nat. Photonics* **2014**, *8*, 506−514.
(2) Meredith, P.; Armin, A. Scaling of next generation solution processed organic and perovskite solar cells. *Nat. Commun.* **2018**, *9*, 5261.
(3) Kang, J.; Wang, L.-W. High Defect Tolerance in Lead Halide Perovskite $CsPbBr_3$. *J. Phys. Chem. Lett.* **2017**, *8*, 489−493.
(4) Walsh, A.; Zunger, A. Instilling defect tolerance in new compounds. *Nat. Mater.* **2017**, *16*, 964−967.
(5) Miyata, K.; Atallah, T. L.; Zhu, X. Y. Lead halide perovskites: Crystal-liquid duality, phonon glass electron crystals, and large polaron formation. *Science Advances* **2017**, *3*, No. e1701469.
(6) Miyata, K.; et al. Large polarons in lead halide perovskites. *Science Advances* **2017**, *3*, No. e1701217.

(7) Frost, J. M.; Walsh, A. What Is Moving in Hybrid Halide Perovskite Solar Cells? *Acc. Chem. Res.* **2016**, *49*, 528−535.
(8) Zhu, H.; et al. Screening in crystalline liquids protects energetic carriers in hybrid perovskites. *Science* **2016**, *353*, 1409−1413.
(9) Zhu, X.-Y.; Podzorov, V. Charge Carriers in Hybrid Organic−Inorganic Lead Halide Perovskites Might Be Protected as Large Polarons. *J. Phys. Chem. Lett.* **2015**, *6*, 4758−4761.
(10) Stranks, S. D.; et al. Electron-Hole Diffusion Lengths Exceeding 1 Micrometer in an Organometal Trihalide Perovskite Absorber. *Science* **2013**, *342*, 341−344.
(11) Wu, B.; et al. Indirect tail states formation by thermal-induced polar fluctuations in halide perovskites. *Nat. Commun.* **2019**, *10*, 484.
(12) Niesner, D.; et al. Structural fluctuations cause spin-split states in tetragonal $(CH_3NH_3)PbI_3$ as evidenced by the circular photogalvanic effect. *Proc. Natl. Acad. Sci. U. S. A.* **2018**, *115*, 9509−9514.
(13) McKechnie, S.; et al. Dynamic symmetry breaking and spin splitting in metal halide perovskites. *Phys. Rev. B: Condens. Matter Mater. Phys.* **2018**, *98*, 085108.
(14) Zheng, F.; Tan, L. Z.; Liu, S.; Rappe, A. M. Rashba Spin−Orbit Coupling Enhanced Carrier Lifetime in $CH_3NH_3PbI_3$. *Nano Lett.* **2015**, *15*, 7794−7800.
(15) Wang, T.; et al. Indirect to direct bandgap transition in methylammonium lead halide perovskite. *Energy Environ. Sci.* **2017**, *10*, 509−515.
(16) Isarov, M.; et al. Rashba Effect in a Single Colloidal $CsPbBr_3$ Perovskite Nanocrystal Detected by Magneto-Optical Measurements. *Nano Lett.* **2017**, *17*, 5020−5026.
(17) Niesner, D.; et al. Giant Rashba Splitting in CH 3 NH 3 PbBr 3 Organic-Inorganic Perovskite. *Phys. Rev. Lett.* **2016**, *117*, 126401.
(18) Röhm, H.; et al. Ferroelectric Properties of Perovskite Thin Films and Their Implications for Solar Energy Conversion. *Adv. Mater.* **2019**, *31*, 1806661.
(19) Monserrat, B.; Vanderbilt, D. Phonon-assisted spin splitting in centrosymmetric crystals. *arXiv:1711.06274 [cond-mat]* (**2017**).
(20) Frohna, K.; et al. Inversion symmetry and bulk Rashba effect in methylammonium lead iodide perovskite single crystals. *Nat. Commun.* **2018**, *9*, 1829.
(21) Zhang, X.; Shen, J.-X.; Wang, W.; Van de Walle, C. G. First-Principles Analysis of Radiative Recombination in Lead-Halide Perovskites. *ACS Energy Letters* **2018**, *3*, 2329−2334.
(22) Azarhoosh, P.; McKechnie, S.; Frost, J. M.; Walsh, A.; van Schilfgaarde, M. Research Update: Relativistic origin of slow electron-hole recombination in hybrid halide perovskite solar cells. *APL Mater.* **2016**, *4*, 091501.
(23) Dar, M. I.; et al. Origin of unusual bandgap shift and dual emission in organic-inorganic lead halide perovskites. *Science Advances* **2016**, *2*, No. e1601156.
(24) Stoumpos, C. C.; et al. Crystal Growth of the Perovskite Semiconductor CsPbBr 3 : A New Material for High-Energy Radiation Detection. *Cryst. Growth Des.* **2013**, *13*, 2722−2727.
(25) Yaffe, O.; et al. Local Polar Fluctuations in Lead Halide Perovskite Crystals. *Phys. Rev. Lett.* **2017**, *118*, 136001.
(26) Thu Ha Do, T.; et al. Optical study on intrinsic exciton states in high-quality CH 3 NH 3 PbBr 3 single crystals. *Phys. Rev. B: Condens. Matter Mater. Phys.* **2017**, *96*, 075308.
(27) Diroll, B. T.; Zhou, H.; Schaller, R. D. Low-Temperature Absorption, Photoluminescence, and Lifetime of $CsPbX_3$ (X = Cl, Br, I) Nanocrystals. *Adv. Funct. Mater.* **2018**, *28*, 1800945.
(28) Sebastian, M.; et al. Excitonic emissions and above-band-gap luminescence in the single-crystal perovskite semiconductors CsPbBr3 and CsPbCl3. *Phys. Rev. B: Condens. Matter Mater. Phys.* **2015**, *92*, 235210.
(29) Yu, Z.-G. Rashba Effect and Carrier Mobility in Hybrid Organic−Inorganic Perovskites. *J. Phys. Chem. Lett.* **2016**, *7*, 3078−3083.
(30) Yu, Z.-G. The Rashba effect and indirect electron−hole recombination in hybrid organic−inorganic perovskites. *Phys. Chem. Chem. Phys.* **2017**, *19*, 14907−14912.
(31) Rakita, Y.; et al. Low-Temperature Solution-Grown CsPbBr3 Single Crystals and Their Characterization. *Cryst. Growth Des.* **2016**, *16*, 5717−5725.
(32) Wright, A. D.; et al. Electron-phonon coupling in hybrid lead halide perovskites. *Nat. Commun.* **2016**, *7*, 11755.
(33) Feynman, R. P. Slow Electrons in a Polar Crystal. *Phys. Rev.* **1955**, *97*, 660−665.
(34) Bychkov, Yu A; Rashba, ÉI. Properties of a 2D electron gas with lifted spectral degeneracy. *JETP Lett* **1984**, *39*, 78.
(35) Monserrat, B.; Vanderbilt, D. Temperature dependence of the bulk Rashba splitting in the bismuth tellurohalides. *Physical Review Materials* **2017**, *1*, 054201.
(36) Covaci, L.; Berciu, M. Polaron Formation in the Presence of Rashba Spin-Orbit Coupling: Implications for Spintronics. *Phys. Rev. Lett.* **2009**, *102*, 186403.
(37) Saidi, W. A.; Poncé, S.; Monserrat, B. Temperature Dependence of the Energy Levels of Methylammonium Lead Iodide Perovskite from First-Principles. *J. Phys. Chem. Lett.* **2016**, *7*, 5247−5252.
(38) Li, Z.; Ma, Z.; Wright, A. R.; Zhang, C. Spin-orbit interaction enhanced polaron effect in two-dimensional semiconductors. *Appl. Phys. Lett.* **2007**, *90*, 112103.
(39) Brivio, F.; et al. Lattice dynamics and vibrational spectra of the orthorhombic, tetragonal, and cubic phases of methylammonium lead iodide. *Phys. Rev. B: Condens. Matter Mater. Phys.* **2015**, *92*, 144308.
(40) Lozhkina, O. A.; et al. Low Inhomogeneous Broadening of Excitonic Resonance in $MAPbBr_3$ Single Crystals. *J. Phys. Chem. Lett.* **2018**, *9*, 302−305.
(41) Iaru, C. M.; Geuchies, J. J.; Koenraad, P. M.; Vanmaekelbergh, D.; Silov, A. Y. Strong Carrier-Phonon Coupling in Lead Halide Perovskite Nanocrystals. *ACS Nano* **2017**, *11*, 11024−11030.
(42) Guo, Y.; et al. Dynamic emission Stokes shift and liquid-like dielectric solvation of band edge carriers in lead-halide perovskites. *Nat. Commun.* **2019**, *10*, 1175.
(43) Milot, R. L.; Eperon, G. E.; Snaith, H. J.; Johnston, M. B.; Herz, L. M. Temperature-Dependent Charge-Carrier Dynamics in $CH_3NH_3PbI_3$ Perovskite Thin Films. *Adv. Funct. Mater.* **2015**, *25*, 6218−6227.
(44) Foley, B. J.; et al. Temperature dependent energy levels of methylammonium lead iodide perovskite. *Appl. Phys. Lett.* **2015**, *106*, 243904.
(45) Saidi, W. A.; Kachmar, A. Effects of Electron−Phonon Coupling on Electronic Properties of Methylammonium Lead Iodide Perovskites. *J. Phys. Chem. Lett.* **2018**, *9*, 7090−7097.
(46) Lautenschlager, P.; Garriga, M.; Logothetidis, S.; Cardona, M. Interband critical points of GaAs and their temperature dependence. *Phys. Rev. B: Condens. Matter Mater. Phys.* **1987**, *35*, 9174−9189.
(47) Bhosale, J.; et al. Temperature dependence of band gaps in semiconductors: Electron-phonon interaction. *Phys. Rev. B: Condens. Matter Mater. Phys.* **2012**, *86*, 195208.
(48) Müller, K. A.; Burkard, H. SrTiO3 : An intrinsic quantum paraelectric below 4 K. *Phys. Rev. B: Condens. Matter Mater. Phys.* **1979**, *19*, 3593−3602.
(49) Rudin, S.; Reinecke, T. L. Temperature-dependent exciton linewidths in semiconductor quantum wells. *Phys. Rev. B: Condens. Matter Mater. Phys.* **1990**, *41*, 3017−3027.
(50) Han, Q.; Wu, W.; Liu, W.; Yang, Q.; Yang, Y. Temperature-dependent photoluminescence of CsPbX3 nanocrystal films. *J. Lumin.* **2018**, *198*, 350−356.
(51) Ramade, J.; et al. Exciton-phonon coupling in a CsPbBr3 single nanocrystal. *Appl. Phys. Lett.* **2018**, *112*, 072104.
(52) Wolf, C.; Lee, T.-W. Exciton and lattice dynamics in low-temperature processable CsPbBr3 thin-films. *Materials Today Energy* **2018**, *7*, 199−207.
(53) Schlipf, M.; Poncé, S.; Giustino, F. Carrier Lifetimes and Polaronic Mass Enhancement in the Hybrid Halide Perovskite CH 3 NH 3 PbI 3 from Multiphonon Fröhlich Coupling. *Phys. Rev. Lett.* **2018**, *121*, 086402.

DOI: 10.1021/acsenergylett.9b01427
ACS Energy Lett. 2019, 4, 2205−2212

(54) Lee, J.; Koteles, E. S.; Vassell, M. O. Luminescence linewidths of excitons in GaAs quantum wells below 150 K. *Phys. Rev. B: Condens. Matter Mater. Phys.* **1986**, *33*, 5512−5516.
(55) Ghosh, S.; et al. Phonon Coupling with Excitons and Free Carriers in Formamidinium Lead Bromide Perovskite Nanocrystals. *J. Phys. Chem. Lett.* **2018**, *9*, 4245−4250.
(56) Zhang, F.; et al. Silica coating enhances the stability of inorganic perovskite nanocrystals for efficient and stable down-conversion in white light-emitting devices. *Nanoscale* **2018**, *10*, 20131−20139.
(57) Han, Q.; Wu, W.; Liu, W.; Yang, Q.; Yang, Y. Temperature-dependent photoluminescence of CsPbX3 nanocrystal films. *J. Lumin.* **2018**, *198*, 350−356.
(58) Lee, S. M.; et al. Temperature-Dependent Photoluminescence of Cesium Lead Halide Perovskite Quantum Dots: Splitting of the Photoluminescence Peaks of $CsPbBr_3$ and $CsPb(Br/I)_3$ Quantum Dots at Low Temperature. *J. Phys. Chem. C* **2017**, *121*, 26054−26062.
(59) Wei, K.; et al. Temperature-dependent excitonic photoluminescence excited by two-photon absorption in perovskite CsPbBr_3 quantum dots. *Opt. Lett.* **2016**, *41*, 3821.
(60) Becker, M. A.; et al. Bright triplet excitons in caesium lead halide perovskites. *Nature* **2018**, *553*, 189−193.
(61) Sercel, P. C.; et al. Exciton Fine Structure in Perovskite Nanocrystals. *Nano Lett.* **2019**, *19*, 4068−4077.
(62) Utzat, H.; et al. Coherent single-photon emission from colloidal lead halide perovskite quantum dots. *Science* **2019**, *363*, 1068−1072.
(63) Tamarat, P.; et al. The ground exciton state of formamidinium lead bromide perovskite nanocrystals is a singlet dark state. *Nat. Mater.* **2019**, *18*, 717−724.

DOI: 10.1021/acsenergylett.9b01427
ACS Energy Lett. 2019, 4, 2205−2212